Journal of Materials Chemistry A

PAPER

View Article Online
View Journal | View Issue

Cite this: J. Mater. Chem. A, 2015, 3, 3059

High-performance lithium–selenium batteries promoted by heteroatom-doped microporous carbon†

Ziqi Yi, Lixia Yuan,* Dan Sun, Zhen Li, Chao Wu, Wenjuan Yang, Yanwei Wen, Bin Shan* and Yunhui Huang*

Received 13th November 2014
Accepted 28th November 2014

DOI: 10.1039/c4ta06141a

www.rsc.org/MaterialsA

A novel microporous N-doped carbon confined Se composite was developed as a cathode material for advanced Li–Se batteries. The microporous N-doped carbon was synthesized by carbonization of a ratio-fixed mixture of polypyrrole and KOH. The Se composite cathode is able to deliver a discharge capacity as high as 303 mA h g^{-1} at 20 C and a reversible capacity of 506 mA h g^{-1} at 1 C, even after 150 cycles. The superior electrochemical performance can be ascribed to the high electrical conductivity promoted by the N-doping and the unique microporous structure of carbonized polypyrrole, which creates additional active sites for Li-ion storage. More importantly, we used a first-principles calculation to evaluate the influence of heteroatom doping on the electrochemical performance, further confirming that the existence of heteroatoms in the carbon framework greatly facilitates the interaction between carbon and Li_2Se, which could well explain the excellent cycling performance and rate capability.

Introduction

Lithium-ion batteries (LIBs) are important options in response to the environmental needs for storage of electrical energy that can be coupled to renewable sources, such as solar and wind. They can also be used as storage for the braking energy of vehicular transport systems. However, given that the traditional insertion cathode materials used in LIBs afford only a limited gravimetric energy density, which cannot meet the requirements of high energy/power density for electric vehicles,[1–3] a new generation of cathode materials with high capacity and energy density is urgently needed. Sulfur is one promising candidate, due to its high theoretical specific capacity (1675 mA h g^{-1}) and theoretical specific energy (2600 W h kg^{-1}), and is usually combined with a Li anode, forming a Li_2S discharge product.[3–8] However, Li–S batteries are plagued by some drawbacks that hinder their practical application, including short cycling lifespan due to dissolution of the intermediate long-chain polysulfides in the electrolyte, and the "shuttle effect" that occurs during the continuous discharge–charge process, which leads to a low coulombic efficiency.[5] Moreover, sulfur presents a low active-material utilization and a poor rate capability, as a result of its insulating nature. In recent years, many approaches have been attempted to address these problems, such as fabricating C–S composites *via* incorporating sulfur into various porous carbon materials to improve the conductivity and to absorb the intermediate polysulfides,[5,9,10] modifying the particle surface[11–14] or cell construction,[15,16] or by adjusting the electrolyte composition to suppress the solubility of the intermediate polysulfides.[17] Although remarkable improvements have been achieved, the realization of Li–S batteries is still hindered by the intrinsic drawbacks of sulfur.

Selenium, as a congener of sulfur, has similar chemical properties with sulfur. Selenium can react with lithium to generate selenide, which can be described by the formula $Se + 2Li^+ + 2e^- \rightarrow Li_2Se$. In spite of its lower specific capacity (about 675 mA h g^{-1}) compared to S (1675 mA h g^{-1}), the volumetric capacity of Se (3253 mA h cm^{-3}, based on 4.82 g cm^{-3}) is comparable to S (3467 mA h cm^{-3}, based on 2.07 g cm^{-3}), as it benefits from a higher density.[18] Moreover, Se possesses an electronic conductivity of 1×10^{-3} S m^{-1}, approximately 20 orders of magnitude higher than S (5×10^{-28} S m^{-1}).[19] Hence, it may be expected that Se could bring about a better rate capability, compared with S. The advantages of Se thus make it a prospective candidate for high-performance rechargeable batteries. In this regard, pioneering work was conducted by Abouimrane *et al.*;[19] they presented a new class of Se cathodes with certain cycling stability. Moreover, Guo *et al.* confined selenium in porous carbon,[18] and were able to achieve a much longer cycle life and better rate performance. Their Se/C cathode could maintain high reversible discharge capacities of 4600 mA h g^{-1}, with a coulombic efficiency of nearly 100%. Liu fabricated nanoporous selenium, using nano-$CaCO_3$ as the

State Key Laboratory of Material Processing and Die and Mould Technology, School of Materials Science and Engineering, Huazhong University of Science and Technology, Wuhan, Hubei 430074, China. E-mail: huangyh@hust.edu.cn; yuanlixia@hust.edu.cn; bshan@hust.edu.cn; Fax: +86 2787558421; Tel: +86 2787558421

† Electronic supplementary information (ESI) available: Details of first principle calculation; TGA curve of the Se–CP composite. See DOI: 10.1039/c4ta06141a

template,[20] and showed it had a higher capacity and better cycling behavior than bulk Se without any treatment.

Analogous to the sulfur system, Li–Se batteries also suffer from fast capacity fading, poor cyclability, and low coulombic efficiency, and it was found that the carbon matrix also plays an important role in Se/C composites, due to its high conductivity, stability, and robust porous structure, which can suppress the diffusion of dissolved polyselenides. To date, the published research is mainly focused on adjusting the morphologies and pore structures of the carbon matrices, while very few reports are concerned with the intrinsic textures of the carbon material. However, the optimization of the carbon material itself can affect the physical and chemical properties of carbon, which can also naturally influence the electrochemical performances of the Se/C composites. Recently, Qu and his group confined selenium in N-containing hierarchical porous carbon and achieved an improvement in rate capability.[21] Zhang *et al.* used nitrogen-doped porous carbon nanofiber webs as an improved carbon matrix for encapsulating selenium.[22] Their corresponding Se/C composite showed good electrochemical performance. The obtained improvements are usually attributed to the interconnected porous nanostructure, the abundant channels structure, and the high specific surface area; however, the heteroatom-doping effect has largely been ignored.

In this work, selenium was confined in N-doped microporous carbon fabricated from carbonized polypyrrole (CP) with KOH as a pore-forming agent. The obtained CP possesses a hierarchical porous structure with regular macropores and interconnected micropores. Nitrogen and oxygen heteroatoms in CP can enhance the chemical adsorption of Li_2Se in the microporous carbon framework, which was verified by a first-principles calculation. The Se–CP cathode shows remarkable cycling performance in carbonate-based electrolytes. At 1 C, the reversible capacity maintains 462 mA h g^{-1} after 150 cycles, with a capacity retention of 70%. Such a Se–CP cathode also exhibits an excellent rate capability. When the current density was increased to 20 C, it delivered a capacity higher than 300 mA h g^{-1}, about half of the theoretical value, thus affording huge advantages in fast discharge–charge applications. The electrochemical performances of the Se–CP cathode in the ether-based electrolyte was also demonstrated.

Experimental

Synthesis of PPy

In a typical procedure, 7.3 g of cetrimonium bromide (CTAB, $(C_{16}H_{33})N(CH_3)_3Br$) was dissolved in 120 mL HCl solution (1 mol L^{-1}), and then cooled down to 0–5 °C. Then, 13.7 g of ammonium persulfate was added; the solution became milky immediately. After being magnetically stirred for 30 min, 8.3 mL pyrrole monomer was added into the as-formed reactive template solution. A black deposit was obtained after stirring for another 24 h. The precipitate was washed with 1 mol L^{-1} HCl solution and deionized water several times until the filtrate became colorless and neutral. It was then dehydrated in an oven at 80 °C.

Synthesis of carbonized PPy (CP)

CP was synthesized by the carbonization of polypyrrole with KOH. Briefly, polypyrrole and KOH were well mixed at a weight ratio of 1 : 3. The mixture was then heated up to 600 °C, at a heating rate of 3 °C min^{-1} for 1 h under a N_2 atmosphere. Then, the solid product was washed with 1 mol L^{-1} HCl solution and deionized water until the filtrated solution became neutral. Then, the sample was dried overnight at 80 °C in an oven.

Synthesis of the composite

To prepare the Se–CP composite, 0.6 g CP and 1.8 g Se were ground together. After being heated at 300 °C for 12 h in a stainless steel autoclave, the obtained composite was transferred to a tube furnace and heated at 350 °C for 2 h to remove residual Se on the surface of the CP.

Material characterization

The XRD patterns were measured on an X-ray powder diffractometer (PANalytical X'pert PRO-DY2198, Holland) operating at 40 kV and 40 mA using Cu Kα radiation ($\lambda = 0.15406$ nm). The morphology of the samples was observed by scanning electron microscope (SEM, SIRION200) and transmission electron microscopy (TEM, JEOL 2100F). Thermogravimetric analyses (TGA, Perkin-Elmer) were carried out in an argon atmosphere at a heating rate of 10 °C min^{-1} from 25 to 1000 °C. The BET surface area, pore size and volume were analyzed using N_2 absorption on a Micromeritics ASAP 2020 analyzer (US). X-ray photoelectron spectroscopy (XPS) was measured by a KRATOS analytical spectrometer (AXIS-ULTRA DLD-600W) using an Al Kα (1486.6 eV) X-ray source. Raman spectra measurements were performed on a Horiba JobinYvon LabRAM HR800.

Electrochemical measurements

The Se–CP electrode was prepared from a mixture of 70 wt% Se–CP composite, 20 wt% super P, 5 wt% carboxy methyl cellulose (CMC), and 5 wt% styrene butadiene rubber (SBR) in deionized water. The homogeneous slurry was coated onto an aluminum foil and dried in a vacuum oven at 60 °C for 24 h. 1 mol L^{-1} of $LiPF_6$ dissolved in a solvent mixture of ethylene carbonate (EC), dimethyl carbonate (DMC), and ethyl methyl carbonate (EMC) (v/v/v = 1 : 1 : 1) or 1 mol L^{-1} LiTFSI dissolved in a solvent mixture of 1,2-dimethoxyethane (DME) and 1,3-dioxolane (DOL) (v/v = 1 : 1) containing 0.1 mol L^{-1} $LiNO_3$ was used as the electrolyte. Li–Se coin cells were assembled in an argon-filled glovebox with oxygen and water contents less than 1 ppm. The as-synthesized Se–CP composite was used as the cathode, metallic lithium foil was used as the anode, and nickel foam was used as the current collector. The capacity and cycle performance were tested at room temperature on a LAND-CT2001A instrument within a voltage range from 1.0 to 3.0 V. Cyclic voltammetry (CV) was measured by an electrochemistry workstation (PARSTAT 2273) between 1.0 and 3.0 V *vs.* Li^+/Li at a scanning rate of 0.1 mV s^{-1}.

Results and discussion

Scheme 1 briefly illustrates the synthesis process for CP and Se–CP composites. Fig. 1a shows the scanning electron microscopy (SEM) image of CP. It exhibits a three-dimensional (3D) architectural structure with macropores on the surface, which can facilitate the mass transport and provide feasible channel access for molten selenium into the micropores of CP. The micropores can be clearly identified by transmission electron microscopy (TEM) (Fig. 1b). After selenium loading, the Se–CP composite maintains a 3D porous structure similar to pure CP and no selenium accumulation can be observed on the surface (Fig. 1c), indicating that selenium is uniformly dispersed and infused into the micropores inside. The energy dispersive X-ray spectroscopy (EDX) image (Fig. 1d) illustrates a high selenium loading in Se–CP. Combined with the TGA result (Fig. S1†), the Se content is determined as 60 wt% in the composite. The peaks of Ca and Si are due to the glass substrate used for the SEM. The Se and C elemental mappings in Fig. 1e indicate that selenium is well-distributed in the Se–CP framework.

In order to further confirm the heteroatoms doping and to investigate the chemical bonding state of functional CP, X-ray photoelectronic spectroscopy (XPS) measurements were carried out. The overall XPS spectrum on CP in Fig. 2a shows three distinct peaks, which represent C 1s, N 1s and O 1s, indicating that the synthesized CP consists of C, N and O. The C 1s (284.7 eV) and N 1s (405.6 eV) peaks are attributed to the carbonization of polypyrrole.[23] The presence of O 1s (531.6 eV) could be assigned to the residual reactant from KOH or the physicochemical adsorption of oxygen during the synthesis. The spectrum of C 1s in CP displayed in Fig. 2b is divided into four individual peaks corresponding to C–C (284.6 eV), C–N (285.4 eV), C–O (286.5 eV), C═O (288.7 eV).[24] It is thus confirmed that the N and O atoms have been successfully doped into the CP. Three characteristic peaks located at 402.1, 400.4 and 398.9 eV (Fig. 2c) match well with the N 1s spectrum, which can be attributed to pyrrolic (N-5), and pyridinic and quaternary N, respectively.[25] This provides evidence that the N atoms within the five-membered ring of PPy have been transformed to N-6 or N-Q partially during the carbonization process. Fig. 2d depicts the XPS survey of the high-resolution O 1s spectrum, indicating that there are several O-based groups, owing to the incorporation of oxygen during the polymerization process of PPy, including C–O–C ether and C–OH phenol groups.[26] The reactivity and electric conductivity can be enhanced by the presence of heteroatoms in CP.[27] The N content in CP can be estimated as 13.28 wt% by the XPS measurement. The XPS results also affirm that the N and O atoms are well introduced into the carbon framework and chemically combine with C, which initiates the asymmetrical charge and spin density of the carbon layer. The resulting charge delocalization in CP provides high conductivity and electrochemical performance.

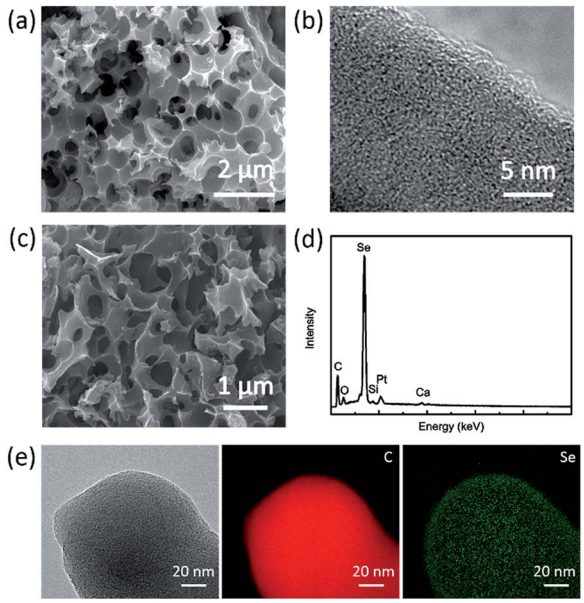

Fig. 1 (a) SEM and (b) TEM images of microporous CP, (c) SEM image and (d) EDX pattern of the Se–CP composite, (e) TEM image of Se–CP composite and the EDX elemental mapping images of carbon and Se in the Se–CP composite.

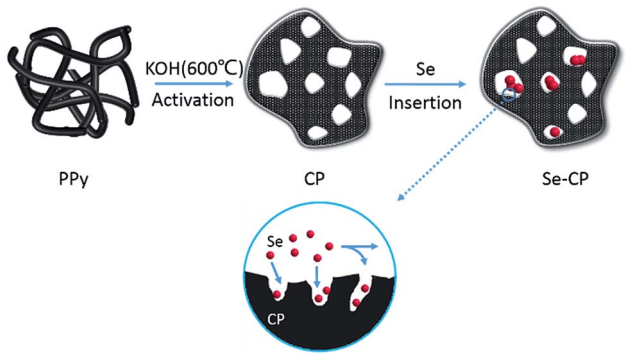

Scheme 1 Schematic illustration of the synthesis procedure of CP and Se–CP composites.

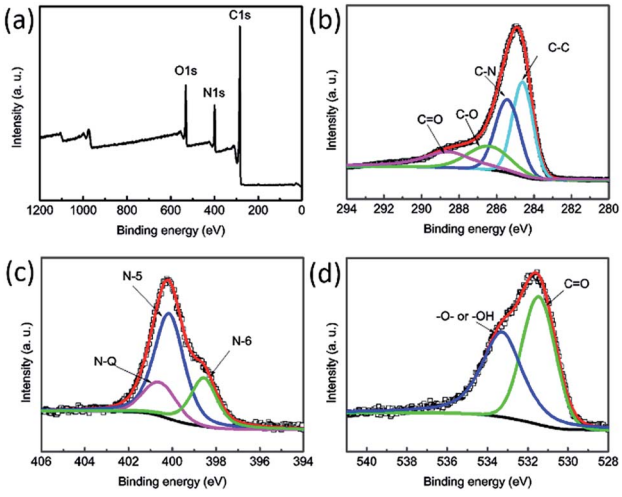

Fig. 2 XPS spectra for CP: (a) survey spectrum, and high-resolution spectra of (b) C 1s, (c) N 1s, and (d) O 1s.

Fig. 3a exhibits the N_2 adsorption–desorption isotherm of the CP. The typical type I isotherm in the low-pressure region and a high fraction of micropores in the pore size distribution curve correspond to the microporous structure of CP. According to the Brunauer–Emmett–Teller (BET) model, the specific surface area is estimated to be 3366 $m^2\ g^{-1}$. This huge surface area can provide sufficient electrode–electrolyte interface for the migration of ions, and hence a high rate performance can be attained. As calculated by the H–K method (Fig. 3b), the obtained CP has an average pore diameter of around 0.5 nm, which agrees well with the TEM image (Fig. 1b). The microporosity of CP is also evidenced by the large pore volume (BJH model) of up to 1.75 $cm^3\ g^{-1}$, demonstrating the extraordinary selenium encapsulation. The amount of rearranging of the Se filler is restricted by the microporous space. In our case, one gram of CP can accommodate 8.4 g of Se. The Se content can be maximized up to 90 wt% if the micropores are fully filled with Se. Since extra space is needed to accommodate the volume expansion caused by the density difference between Se and the discharge product Li_2Se, the Se content in Se–CP is selected at 60 wt%, as further determined by the thermogravimetric analysis (TGA), as shown in Fig. S1.†

The XRD patterns of CP and Se–CP are shown in Fig. 4. In Fig. 4a, a broad (002) peak appears in both CP and Se–CP, which is indicative of the amorphous state for carbon. No peaks of Se are observed in the Se–CP composite, demonstrating that Se exists in a highly dispersed amorphous state. To better understand the interaction between Se and CP, the Raman spectra of bulk Se, CP and Se–CP are compared in Fig. 4b. For pure Se, three peaks are observed, among which the peaks at 142.5 cm^{-1} and 458.6 cm^{-1} represent annular Se, while the 236.6 cm^{-1} peak represents the chain-structured Se.[28] It can be inferred that pure Se is a mixture of annular Se and chain-structured Se.[29] As for CP, the peak at 1333 cm^{-1} (D-band) is attributed to some imperfections like defects, disorders or impurities, while the G-band at 1595 cm^{-1} arises from the lattice vibration of graphitic carbon. The graphitization degree of the carbon material is usually evaluated according to the intensity ratio of I_D to I_G. However, as evaluated from the Raman spectra, the I_D/I_G ratio for the as-obtained CP is about 0.95, further verifying its partial graphitization degree. Graphitization can ensure good electronic conductivity and facilitate electron transport, and thus can result in a good electrochemical performance. After the encapsulation of Se into the microporous structured CP, the intensity of the typical Se peaks dramatically decreases,

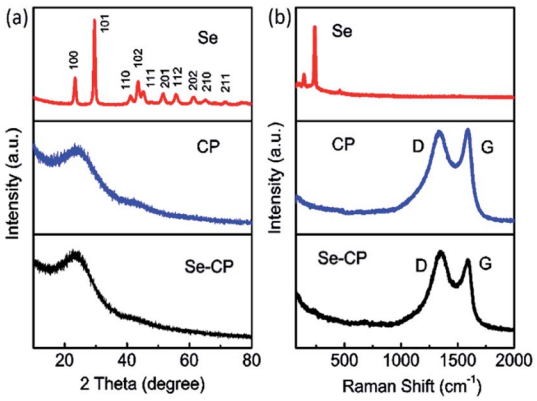

Fig. 4 (a) XRD patterns and (b) Raman spectra of Se, CP, and Se–CP.

indicating that amorphous Se is embedded successfully into the pores of CP, which agrees well with the XRD patterns.[18,29] According to the equation for the graphitization degree,[30] no peak shift is observed in Se–CP, but a slight increase occurs in the I_D/I_G ratio, which may be ascribed to the interaction between the incorporated Se with some unsaturated chemical bonds in CP.

The electrochemical properties were evaluated by coin cells with the lithium anode and the as-synthesized Se–CP cathode in both ether- and carbonate-based electrolytes. CV testing was conducted to investigate the kinetics process during discharge and charge. Fig. 5a shows the CV curves of the 1st, 2nd and 5th cycles in ether-based electrolyte at a scan rate of 0.1 mV s^{-1} from 1.0 to 3.0 V. The first cycle shows several ambiguous peaks and one sharp anodic peak at 2.32 V, which is related with not only the reduction and oxidation of Se, but also with the activation process of the cathode and some side reactions between the electrolyte and cathode as well.[31] In the subsequent cycles, three cathodic peaks at 2.17, 2.08 and 1.82 V indicate the conversion of elemental Se to Li_2Se *via* a multiple-phase change. Similar to the sulfur system, during lithiation, Se is reduced to soluble long-chain polyselenides Se_n^{2-} ($n \geq 4$), and then further reduced to Li_2Se in the following process. In the delithiation process, the three anodic peaks located at 2.04, 2.13 and 2.32 V correspond to the oxidation of Li_2Se to Se with the formation of intermediate Se_n^{2-} ($n \geq 4$). Obviously, the Se cathode also suffers from the dissolution issue of polyselenides in the ether electrolyte during the charge and discharge process. Unlike the

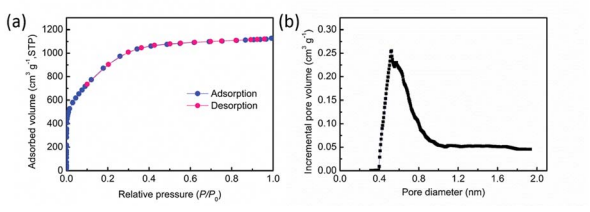

Fig. 3 (a) Nitrogen adsorption–desorption isotherms, and (b) the pore size distribution of CP.

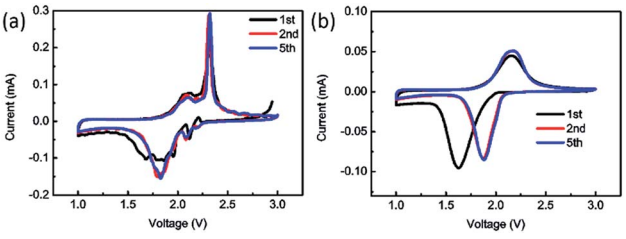

Fig. 5 Cyclic voltammograms of Se–CP composite in (a) ether and (b) carbonate-based electrolyte during the 1st, 2nd, and 5th cycles.

case in the ether-based electrolyte, the CV curves of the Se–CP cathode in the carbonate-based electrolyte (Fig. 5b) reveal a strong reduction peak at 1.65 V and an oxidation peak at 2.2 V in the first cycle. Interestingly, the cathodic peak shifts to a higher potential in the following cycling and is stabilized at 1.9 V, with the anodic peak remaining at 2.2 V. This phenomenon is ascribed to the deformation of the Se–CP cathode, caused by lithiation in the first cycle. In addition, for the redox process of Se–CP in the carbonate-based electrolyte, only one reduction peak and one oxidation peak can be observed. It seems that there is no soluble Li_2Se_n ($n \geq 4$) formed during the reaction, and that only a direct phase change occurs between Se and Li_2Se, which agrees well with Yang's results.[18] Unlike the composites of sulfur confined in the microporous carbon, which always show a much lower discharge plateau in the carbonate-based electrolyte than that in the ether-based electrolyte,[10,32] the Se–CP cathode in the carbon-based electrolyte shows a similar reduction potential (1.9 V) to that in the ether-based electrolyte. Furthermore, after the initial activation process, the redox curves of the Se–CP cathode in the carbonate-based electrolyte becomes very stable, indicative of a good reversibility, which could be attributed to the excellent ability of CP to confine and stabilize both Se and Li_2Se during the electrochemical process.

The discharge–charge performance of the Se–CP composite was investigated in both ether- and carbonate-based electrolyte (Fig. 6). Fig. 6a shows the discharge–charge profiles of the typical cycles. The Se–CP composite exhibits a very high capacity of 1504 mA h g^{-1} in the first discharging process, and a reversible capacity of 480 mA h g^{-1}. A high irreversible capacity in the first cycle is commonly observed in Li–S and Li–Se cells when porous carbon is used as the support,[18] which mainly arises from the irreversible reactions between the porous carbon and the electrolyte. For the ether electrolyte system, there is a little fluctuation with the coulombic efficiency in the initial 20 cycles (Fig. 6b), but this remains stable in the following cycles. A reversible capacity of 413 mA h g^{-1} is attained after 50 cycles. A higher reversible capacity and better cycle performance are achieved in the carbonate-based electrolyte. In the carbonate-based electrolyte, the Se–CP cathode shows a much higher initial reversible capacity of 664 mA h g^{-1} (Fig. 6c); even after 150 cycles, a reversible capacity of 506 mA h g^{-1} still remains, together with a coulombic efficiency of nearly 100% (Fig. 6d). For the Se–CP cathode in the carbonate-based electrolyte, a remarkable rate capability is also achieved (Fig. 6e and f). When the current density increases rapidly from 0.5 C to 20 C, the discharge capacity drops slowly. At 20 C, the discharge capacity of Se–CP still reaches up to 303 mA h g^{-1}. When the current density is turned back to 0.5 C after cycling at various rates, a reversible capacity of 577 mA h g^{-1} can be recovered. The excellent capacity retention and rate capability could be attributed to the excellent electronic conductivity of Se–CP, which facilitates electron transport, and hence results in a low polarization.

The excellent electrochemical performance for Se–CP can also be related to the heteroatoms doping. Nitrogen shows an electronegativity of 3.5, which is much higher than that of

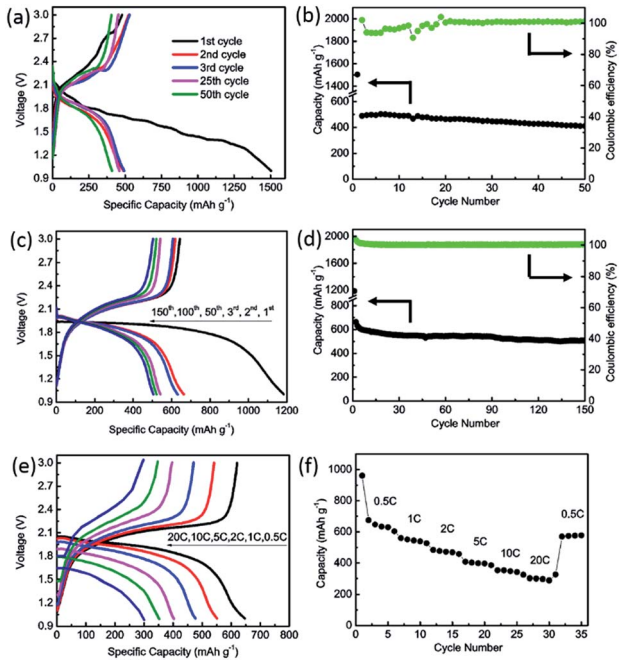

Fig. 6 Electrochemical performances of the Se–CP composite: (a) charge–discharge profiles in the 1st, 2nd, 3rd, 25th, and 50th cycle; and (b) cycling performance and coulombic efficiency in the ether-based electrolyte at 1 C; (c) charge–discharge profiles in the 1st, 2nd, 3rd, 50th, 100th, and 150th cycle; and (d) cycling performance and coulombic efficiency in the carbonate-based electrolyte at 1 C, (e) charge–discharge profiles at different currents, and (f) rate capability at various rates from 0.5 to 20 C in the carbonate-based electrolyte.

carbon (3.0); however, the nitrogen atom is smaller than the carbon atom, and therefore N-doping can facilitate lithium insertion[33] and strengthen the interaction between the carbon host and lithium selenide. To elucidate more about the importance of N-doping, we modeled and calculated the binding energy of the carbon framework with and without heteroatoms by a first-principles calculation. Although this simulation cannot give a precise quantification of the binding strength, it can provide a qualitative understanding of the influence of the chemical bonds on the cycling stability and rate capability for Se–CP. Fig. 7 depicts a brief carbon layer with partial N-doping, in which O-1 and O-2 come from the hydroxyl and carbonyl groups, respectively. We computed the binding energy of CP with the particles involved in the electrode

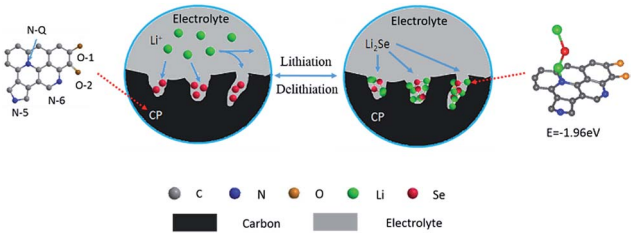

Fig. 7 Schematic illustration of the charge and discharge mechanism and the carbon framework model for the first-principles calculation.

Table 1 Binding energy of different atoms in CP with Li^+ and Se calculated by first principles[a]

Structure	N-5 with Se	N-6 with Se	N-Q with Se	O-1 with Se	O-2 with Se	C with Se
Energy/eV	−5.47	−2.54	−3.29	−4.36	−2.53	−2.25
Structure	N-5 with Li^+	N-6 with Li^+	N-Q with Li^+	O-1 with Li^+	O-2 with Li^+	C with Li^+
Energy/eV	−3.92	−4.32	−4.17	−4.2	−4.32	−3.51

[a] More calculation details are provided in the ESI.

reactions *via* first-principles calculation according to the equation described as:

$$E = E_{total} - E_{CP} - E_X \ (X = Se, Li^+, Li_2Se)$$

Further details on the calculation are provided in the ESI.† The calculated results are summarized in Table 1. We can see that the heteroatoms have a stronger interaction with Se atoms and lithium ions to form a chelated coordination structure. This strong binding affinity contributed by the doped heteroatoms can effectively enhance the reaction kinetics and facilitate the electrode reaction. Fig. 7 illustrates the interaction between the carbon framework and Li_2Se. We selected a position where Li_2Se could bond with CP to determine the interaction. The binding energy was found to increase from 1.51 to 1.96 eV after specific carbon positions were replaced by heteroatoms (N-doped), from which we can conclude that the special N-doping structure can suppress the Li_2Se extraction, which can give rise to excellent cycling stability.

Conclusions

A novel Se composite confined in an N-doped microporous carbon was successfully designed and fabricated *via* a facile melting-diffusion route. As a cathode material for the Li–Se battery, the Se–CP composite possesses high stability in low-cost commercial carbonate-based electrolyte and exhibits remarkable cycle stability and rate capability. A high reversible capacity of 462 mA h g^{-1} can be attained at 1 C, even after 150 cycles. Combined with a first-principles modeling calculation, we ascribe the outstanding performances to the following reasons: (1) the partially graphitized carbon with micropores and a large surface area and high conductivity can facilitate the electron transfer and Li-ion diffusion; (2) the robust microstructure can effectively confine the Se species during the discharging and charging process, promoting high stability of the electrode structure; and (3) more importantly, the doping of the heteroatoms N and O in carbon greatly enhances the binding energy between the carbon and Se or Li_2Se, resulting in high electrochemical performance.

Acknowledgements

This work was supported by the Natural Science Foundation of China (Grant nos 21273087 and 51361130151) and the 973 program (Grant nos 2015CB258400). In addition, the authors thanks the Analytical and Testing Center in Huazhong University of Science and Technology for XRD, SEM, TEM, XPS measurement, and the State Key Laboratory of Material Processing and Die and Mould Technology for TGA measurements.

References

1 P. G. Bruce, S. A. Freunberger, L. J. Hardwick and J. M. Tarascon, *Nat. Mater.*, 2012, **11**, 19.
2 B. L. Ellis, K. T. Lee and L. F. Nazar, *Chem. Mater.*, 2010, **22**, 691.
3 X. Ji and L. F. Nazar, *J. Mater. Chem.*, 2010, **20**, 9821.
4 J. Shim, K. A. Striebel and E. J. Cairns, *J. Electrochem. Soc.*, 2002, **149**, A1321.
5 X. Ji, K. T. Lee and L. F. Nazar, *Nat. Mater.*, 2009, **8**, 500.
6 B. Jin, J.-U. Kim and H.-B. Gu, *J. Power Sources*, 2003, **117**, 148.
7 S. Wei, H. Zhang, Y. Huang, W. Wang, Y. Xia and Z. Yu, *Energy Environ. Sci.*, 2011, **4**, 736.
8 Y. Yang, M. T. McDowell, A. Jackson, J. J. Cha, S. S. Hong and Y. Cui, *Nano Lett.*, 2010, **10**, 1486.
9 S. H. Chung and A. Manthiram, *Adv. Mater.*, 2014, **26**, 1360.
10 S. Xin, L. Gu, N. H. Zhao, Y. X. Yin, L. J. Zhou, Y. G. Guo and L. J. Wan, *J. Am. Chem. Soc.*, 2012, **134**, 18510.
11 W. Li, G. Zheng, Y. Yang, Z. W. Seh, N. Liu and Y. Cui, *Proc. Natl. Acad. Sci. U. S. A.*, 2013, **110**, 7148.
12 Y. Fu, Y.-S. Su and A. Manthiram, *Adv. Energy Mater.*, 2014, **4**, 1300655.
13 Z. Wei Seh, W. Li, J. J. Cha, G. Zheng, Y. Yang, M. T. McDowell, P. C. Hsu and Y. Cui, *Nat. Commun.*, 2013, **4**, 1331.
14 W. Li, Q. Zhang, G. Zheng, Z. W. Seh, H. Yao and Y. Cui, *Nano Lett.*, 2013, **13**, 5534.
15 Y. S. Su and A. Manthiram, *Nat. Commun.*, 2012, **3**, 1166.
16 C. Huang, J. Xiao, Y. Shao, J. Zheng, W. D. Bennett, D. Lu, L. V. Saraf, M. Engelhard, L. Ji, J. Zhang, X. Li, G. L. Graff and J. Liu, *Nat. Commun.*, 2014, **5**, 3015.
17 Z. Lin, Z. Liu, W. Fu, N. J. Dudney and C. Liang, *Adv. Funct. Mater.*, 2013, **23**, 1064.
18 C.-P. Yang, S. Xin, Y.-X. Yin, H. Ye, J. Zhang and Y.-G. Guo, *Angew. Chem., Int. Ed.*, 2013, **52**, 8363.
19 A. Abouimrane, D. Dambournet, K. W. Chapman, P. J. Chupas, W. Weng and K. Amine, *J. Am. Chem. Soc.*, 2012, **134**, 4505.
20 L. Liu, Y. Hou, X. Wu, S. Xiao, Z. Chang, Y. Yang and Y. Wu, *Chem. Commun.*, 2013, **49**, 11515.
21 Y. Qu, Z. Zhang, S. Jiang, X. Wang, Y. Lai, Y. Liu and J. Li, *J. Mater. Chem. A*, 2014, **2**, 12255.

22 J. Zhang, Z. Zhang, Q. Li, Y. Qu and S. Jiang, *J. Electrochem. Soc.*, 2014, **161**, A2093.
23 C. Malitesta, I. Losito, L. Sabbatini and P. G. Zambonin, *J. Electron Spectrosc. Relat. Phenom.*, 1995, **76**, 629.
24 Y. Li, Y. Zhao, H. Cheng, Y. Hu, G. Shi, L. Dai and L. Qu, *J. Am. Chem. Soc.*, 2012, **134**, 15.
25 L. F. Chen, X. D. Zhang, H. W. Liang, M. Kong, Q. F. Guan, P. Chen, Z. Y. Wu and S. H. Yu, *ACS Nano*, 2012, **6**, 7092.
26 D. Hulicova-Jurcakova, M. Seredych, G. Q. Lu and T. J. Bandosz, *Adv. Funct. Mater.*, 2009, **19**, 438.
27 L. Qie, W. M. Chen, Z. H. Wang, Q. G. Shao, X. Li, L. X. Yuan, X. L. Hu, W. X. Zhang and Y. H. Huang, *Adv. Mater.*, 2012, **24**, 2047.
28 R. Lukács, M. Veres, K. Shimakawa and S. Kugler, *J. Appl. Phys.*, 2010, **107**, 073517.
29 C. Luo, Y. Xu, Y. Zhu, Y. Liu, S. Zheng, Y. Liu, A. Langrock and C. Wang, *ACS Nano*, 2013, **7**, 8003.
30 J. L. K. F. Tuinstra, *J. Compos. Mater.*, 1970, **4**, 492.
31 Y. Cui, A. Abouimrane, J. Lu, T. Bolin, Y. Ren, W. Weng, C. Sun, V. A. Maroni, S. M. Heald and K. Amine, *J. Am. Chem. Soc.*, 2013, **135**, 8047.
32 Z. Li, L. X. Yuan, Z. Q. Yi, Y. M. Sun, Y. Liu, Y. Jiang, Y. Shen, Y. Xin, Z. L. Zhang and Y. H. Huang, *Adv. Energy Mater.*, 2014, **4**, 1301473.
33 Y. P. Wu, C. Y. Jiang, C. R. Wang, S. B. Fang and Y. Y. Jiang, *J. Appl. Polym. Sci.*, 2000, **77**, 1735.